Effects of rejuvenation modes on the microstructures and mechanical properties of metallic glasses

Shan Li [a], Yue Yu [b], Paulo S. Branicio [c,*], Zhen-Dong Sha [a,d,*]

[a] State Key Laboratory for Strength and Vibration of Mechanical Structures, School of Aerospace Engineering, Xi'an Jiaotong University, Xi'an 710049, China

[b] College of pharmacy, Nanjing University of Chinese Medicine, 138 Xianlin Road, Nanjing 210028, China

[c] Mork Family Department of Chemical Engineering and Materials Science, University of Southern California, 3651 Watt Way, Los Angeles, CA 90089, United States

[d] State Key Laboratory of Nonlinear Mechanics, Institute of Mechanics, Chinese Academy of Sciences, Beijing 100190, China

Abstract

This study systematically investigates the effects of three rejuvenation modes, namely biaxial loading, thermal pressure loading, and cryogenic thermal cycling, on the microstructures and mechanical properties of $Cu_{64}Zr_{36}$ metallic glasses (MGs) using molecular dynamics (MD) simulations. The simulation results demonstrate that biaxial tension application during loading results in a rejuvenated glassy state with high strength. Specifically, we find that the yield stress, Young's modulus, and shear modulus of the rejuvenated glass obtained by biaxial tensile loading decreased by 2.8%, 2.1%, and 2.7%, respectively, compared to an as-cast MG reference. We also find that MGs achieve the greatest degree of rejuvenation, at the expense of strength, with the use of thermal pressure loading. Interestingly, the application of cryogenic thermal cycling results in a rejuvenated state with a lower strength drop compared to thermal pressure loading. Furthermore, analysis of the potential energy and medium-range-order (MRO) size indicates that the microstructures of MGs achieves a high-energy ordered glass state after thermal pressure loading, but a high-energy disordered glass state after

* Corresponding authors.
E-mail address: branicio@usc.edu (P.S. Branicio), zhendongsha@mail.xjtu.edu.cn (Z.-D. Sha)

biaxial tensile loading and cryogenic thermal cycling. These findings provide meaningful insights into the effect of rejuvenation modes on the microstructures and mechanical properties of MGs, as well as useful guidelines for designing MGs with high strength and superior plasticity for prospective applications in industry.

Keywords

Metallic glass; Rejuvenation method; Mechanical property; Amorphous microstructures

1. Introduction

The Metallic glass (MGs) exist in an out-of-equilibrium configuration at room temperature and tend to spontaneously move towards a more stable, low-energy state through a process called physical aging [1]. As this process occurs, the physical and mechanical properties of MGs tend to deteriorate [1]. Conversely, the rejuvenation of MGs is a process that operates in the opposite direction of aging, whereby the material is transformed into a higher energy state, leading to an enhancement in deformability at room temperature [2-4]. Rejuvenation leads to structural changes in the MGs, resulting in a transition from localized shear banding to homogeneous plastic deformation, thereby making it possible to create high-strength and high-toughness MG based materials. This property makes rejuvenation an extremely attractive process for developing high-performance materials.

Previous studies have reported that mechanical methods [2, 5-7], irradiation [4, 8] or thermal treatment [9, 10] can be utilized to rejuvenate MGs. However, the use of such methods can also induce internal stress in the material, which significantly reduces its ultimate strength [2, 5]. The “irradiation rejuvenation” region with gradient structure increases the tensile ductility of MGs, leading to a change of deformation mode from brittle to ductile [4]. Nonetheless, ion radiation is a localized process making it challenging to effectively rejuvenate the entire MG sample [8]. In this regard, thermal

treatment rejuvenation of MGs has garnered significant attention. Wakeda *et al.* have demonstrated that pure thermal treatment can rejuvenate MGs, provided that two conditions are satisfied simultaneously: the cooling rate following isothermal annealing must be higher than that of the quenching process, and the annealing temperature must exceed the critical temperature [9]. More recently, Sohrabi *et al.* have demonstrated that cryogenic thermal cycling is able to rejuvenate low-purity $La_{60}Al_{25}Ni_{15}$ MGs, resulting in their transition from brittle to ductile deformation behavior [8].

Numerous studies have provided valuable insights into understanding the effect of rejuvenation on the MG. However, the microstructures and mechanical properties of MGs resulting from the application of various rejuvenation modes is still left to be properly characterized and understood. Therefore, it is necessary to select the most representative rejuvenation modes and critically compare their effects.

In general, mechanical rejuvenation modes, such as shot peening [11], wire drawing [12], high-pressure torsion [2], and uniaxial elastostatic loading [13, 14] introduce a high density of localized shear bands through severe plastic deformation. Thus, mechanical rejuvenation is characterized by localized rejuvenation and severe shape changes. Uniaxial elastostatic loading has emerged as a promising approach to overcome the drawbacks of traditional mechanical rejuvenation. For instance, Park *et al.* conducted uniaxial elastostatic compression of CuZr MGs at room temperature and observed homogeneous rejuvenation throughout the entire sample [13]. Furthermore, Tong *et al.* reported that anelastic creep strain, as opposed to plastic strain, can induce structural rejuvenation in MGs [14].

In comparison to mechanical rejuvenation modes, various thermal treatment methods have been proposed, including pure thermal treatment [9], thermal pressure loading [15-17], and cryogenic thermal cycling [10, 18]. Li *et al.* demonstrated, through simulations, that thermal pressure-induced rejuvenation in MGs can mitigate their inherent brittleness while preserving their high strength [15]. Moreover, Miyazaki *et al.* reported that isothermal annealing followed by cooling at a rate equal to the quenching process can lead to rejuvenation and result in higher strength than pure thermal

treatment [17]. Cryogenic thermal cycling is an energy-efficient and non-destructive method that effectively enhances the mechanical properties of MGs [18]. Ketov *et al.* revealed that the rejuvenation effects of cryogenic thermal cycling are dependent on the cycle number, holding time, and chemical composition [18]. Their experimental observations suggest that cryogenic thermal cycling can achieve rejuvenation of MGs, which is attributed to their non-uniform thermal expansion coefficient.

In this work, we investigate the impact of three promising rejuvenation modes, namely biaxial loading, thermal pressure loading, and cryogenic thermal cycling, on the microstructures and mechanical properties of MGs. We employ molecular dynamics (MD) simulations, with the aim of unveiling novel insights into the rejuvenation mechanisms of MGs, which can pave the way for designing high-strength and high-toughness materials. Our work fills a gap in the literature, as the critically compared effect of rejuvenation modes on the microstructures and mechanical properties of MGs is still to be discussed. We expect our results can be leveraged to advance the field of MGs and inspire further investigations.

2. Simulation methods

All MD simulations in this work employs LAMMPS [19]. The pressure and temperature in the simulations are controlled by Parrinello-Rahman barostat and a Nose-Hoover thermostat, respectively. The simulated system is a nanoscale $Cu_{64}Zr_{36}$ MG sample containing approximately 0.43 million atoms arranged in a slab with dimensions of 24.4 (x) × 48.8 (y) × 6.1 (z) nm^3. An embedded atom method (EAM) potential tailored to CuZr alloys is utilized to describe the interatomic interactions [20]. A constant integration timestep of 2 fs is used in all MD simulations. To create the large $Cu_{64}Zr_{36}$ MG sample, a smaller sample (~13,000 atoms) with periodic boundary conditions (PBCs) along all three independent directions is initially equilibrated at a temperature of 2000 K for 2 ns, and then rapidly cooled at a quenching rate of 1 K/ps to a temperature of 300 K at zero external pressure. The large MG sample is built by replications of the small MG sample, which is then annealed at 800 K above the glass

transition temperature for 1 ns to minimize artificial patterns introduced during the replication process. During the replication procedure, PBCs are applied in all three dimensions and the quenching rate is the same as that used in the preparation of small MG samples. The constructed large MG sample is hereafter referred to as the 'as-cast MG'.

Subsequently, the as-cast MGs undergo thermal pressure loading, biaxial tensile loading, and cryogenic thermal cycling. The thermal pressure loading process is illustrated in Fig. 1(a). The applied pressure P_a is set to 3 GPa, and the annealing temperature T_a is set either at 800 K, 900 K, or 1000 K. Both the heating rate (A→B) and cooling rate (C→D) are 1 K/ps. The glass transition temperature T_g = 650 K is determined by the intersection point of the volume-temperature curve for the glassy and liquid states [15].

Figure 1(b) depicts the biaxial tensile loading process. The as-cast MGs are subjected to a chosen stress σ_c (A→B in Fig. 1(b)), which is held constant for 20 ns (B→C), followed by unloading (C→D), and finally relaxation for 5 ns (D→E). For biaxial loading, a constant tensile stress is applied instantaneously in the *x*- and *y*-directions, while the ambient pressure is maintained in the *z*-direction. The biaxial loading stresses (σ_c) employed in this study are 2.3 GPa, 2.4 GPa, 2.5 GPa, and 2.6 GPa, respectively. All post processing is conducted at room temperature, and the chosen loading stresses are below the yield stress (σ_y = 2.9 GPa). In the present work, different applied pressures are utilized for thermal pressure loading and biaxial loading. It is because that the focus of thermal pressure loading is primarily on the high-pressure environment, while the high pressure condition is not necessary for rejuvenation in the case of biaxial loading.

Figure 1(c) illustrates the cryogenic thermal cycling process. We set the upper temperature to 400 K, the lower temperature to 10 K, and the cycle number (CN) to 40. The hold times at lower and upper temperatures are t_1 = 100 ps and t_2 = 10 ps, respectively. Wang *et al.* have reported that the selection of holding time (t_1 and t_2) has no obvious effect on the results of cryogenic thermal cycling [18]. The heating rate and

cooling rate are both 1 K/ps.

The MG samples obtained through the aforementioned three rejuvenation modes are referred to as 'post-processed MGs' throughout this study. After post processing, uniaxial tensile tests are conducted on the as-cast and post-processed MGs at room temperature. During the uniaxial tensile tests, PBCs are imposed in the *y*- and *z*-directions, while the free surface condition is utilized along the *x*-direction. We employ a constant tensile strain rate of 10^8 s^{-1} along the *y*-direction.

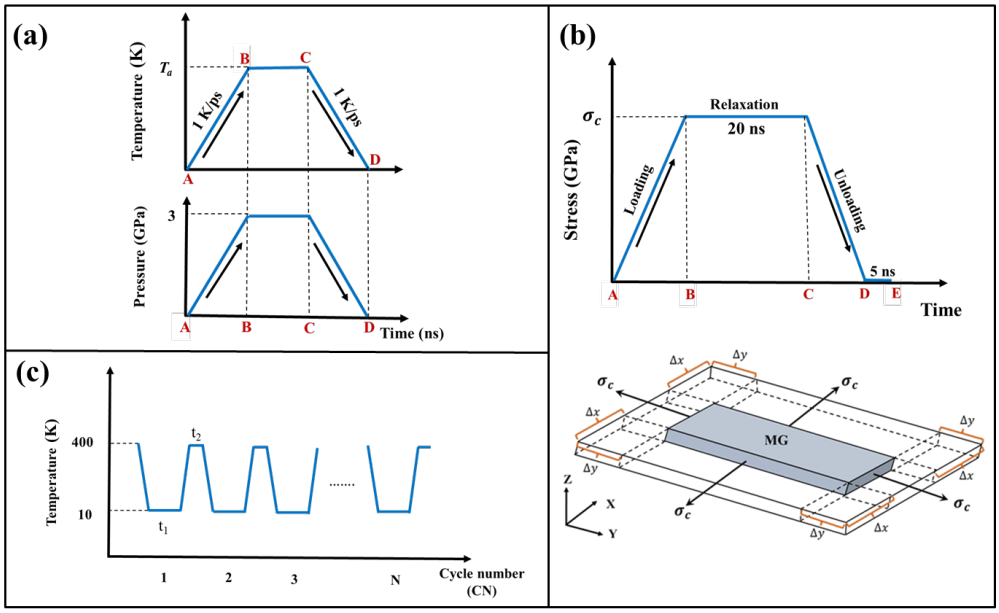

Fig. 1. Schematics of the $Cu_{64}Zr_{36}$ MG samples loading processes. (a) Illustration of the thermal pressure loading. (b) Illustration of the biaxial tensile loading at room temperature, where Δx and Δy represent the elongation after post processing in the *x*- and *y*-directions, respectively. (c) Illustration of the cryogenic thermal cycling process.

3. Results and discussions

3.1. Potential energy

Compared to as-cast MGs, post-processed MGs exhibit changes in their potential energy. A positive potential energy change (ΔE) indicates rejuvenation of the MG, while a negative ΔE indicates aging [15]. Fig. 2(a)-(c) present the ΔE values of $Cu_{64}Zr_{36}$ MGs after undergoing thermal pressure loading, biaxial tensile loading, and cryogenic thermal cycling, respectively. As shown in Fig. 2(a), when the annealing temperature

(T_a) is 800 K, the ΔE is negative, indicating that the $Cu_{64}Zr_{36}$ MGs is aging. On the other hand, when T_a is 900 K and 1000 K, the ΔE is positive, indicating that rejuvenation is achieved. It is well established that thermal pressure loading can rejuvenate MGs at annealing temperatures $T_a \geq 1.3T_g$ [15]. Thus, rejuvenation in $Cu_{64}Zr_{36}$ MGs can only occur at $T_a \geq 845$ K, which is consistent with our simulation results.

In Fig. 2(b), it is evident that the potential energy change of the post-processed MGs is dependent on the loading stress, σ_c, i.e., when the loading stress σ_c = 2.3 GPa, ΔE < 0, indicating MG aging, however, when the loading stress σ_c = 2.4 GPa, ΔE > 0, indicating MG rejuvenation. Additionally, it can be observed that the magnitude of ΔE increases with an increase in loading stress. It is well-established that the degree of rejuvenation of MGs with the same composition is proportional to the ΔE value [17]. Nevertheless, at loading stress levels approaching the yield stress (σ_y), there is a risk of inhomogeneous plastic flow [21]. Therefore, for biaxial tensile loading rejuvenation, the appropriate loading stress must be carefully chosen. The maximum loading stress chosen for this study is 2.6 GPa, which does not cause shear banding and can rejuvenate the MG.

Figure 2(c) illustrates an increase in ΔE with the cycle number until it stabilizes at a positive value. When CN = 15, ΔE is positive, but the degree of rejuvenation is insufficient. The magnitude of ΔE continues to increase as the cycle number rises, with the value tending towards stability after 20 cycles. The occurrence of rejuvenation through cryogenic thermal cycling is surprising due to the small macroscopic strains and temperatures significantly below those that trigger thermally induced structural changes. The reason for the potential energy change caused by this method is that after several cycles, the local rearrangement of atoms gradually replaces the original glass microstructures [22]. This phenomenon is closely linked to the heating stage of each thermal cycle and the inhomogeneity of the local thermal expansion coefficient of the MG samples [22]. In fact, the impact of cycle number on the potential energy of MGs is highly complex, and MGs with differing chemical compositions may display

completely different behaviors [23].

Based on the above analysis, it can be inferred that thermal pressure loading, biaxial tensile loading, and cryogenic thermal cycling have varying impacts on the ΔE of MGs. When T_a = 1000 K, thermal pressure loading yields a ΔE of 0.01 eV/atom, while biaxial tensile loading with a stress of 2.6 GPa results in a ΔE of 0.0021 eV/atom. On the other hand, cryogenic thermal cycling leads to a stable positive value of ΔE as the cycle number increases, with ΔE ≈ 0.0012 eV/atom. The analysis indicates that the highest ΔE value for $Cu_{64}Zr_{36}$ MGs is achieved after thermal pressure loading, implying it achieves the most significant degree of rejuvenation.

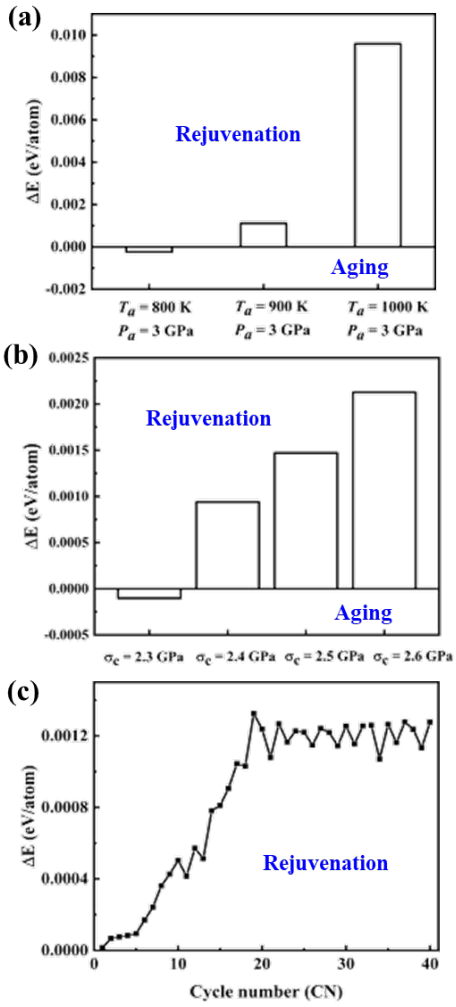

Fig. 2. Potential energy change (ΔE) of $Cu_{64}Zr_{36}$ MG induced by different loading processes. (a) Thermal pressure loading, (b) biaxial tensile loading, and (c) cryogenic thermal cycling.

3.2. Thermal pressure loading

3.2.1. Mechanical properties

Figure 3(a) shows the tensile stress-strain curves for the post-processed MG at various annealing temperatures, along with the curve for the as-cast MGs for comparison. It is observed that at T_a = 800 K, the yield stress (σ_y) remains nearly unchanged. However, the flow stress (σ_f) exhibits a sharp decrease with increasing tensile strain, indicating the formation of mature shear bands in the $Cu_{64}Zr_{36}$ MGs [24]. At T_a = 900 K, the yield stress decreases slightly, and the decrease in flow stress with increasing tensile strain is less pronounced, implying a change in the plastic deformation behavior of $Cu_{64}Zr_{36}$ MGs. At T_a = 1000 K, the yield stress experiences a significant decline, followed by a slowed decrease in flow stress, also indicating a change in the deformation mechanism of $Cu_{64}Zr_{36}$ MGs. These results indicate that as the annealing temperature increases, the yield stress decreases. Further insight into the deformation mechanism is presented in Fig. 3(b).

Figure 3(b) displays a series of snapshots that illustrate the deformation of both as-cast and post-processed MGs. The as-cast MG exhibits catastrophic failure, with evident shear banding. At an annealing temperature of T_a = 800 K, two mature shear bands interact, leading to necking of the MGs and eventual failure of the material. At annealing temperatures of T_a = 900 K and T_a = 1000 K, no mature shear band formation is observed, and the shear strain is uniformly distributed throughout the sample, indicating a change in the deformation mechanism of the MGs from brittle to ductile.

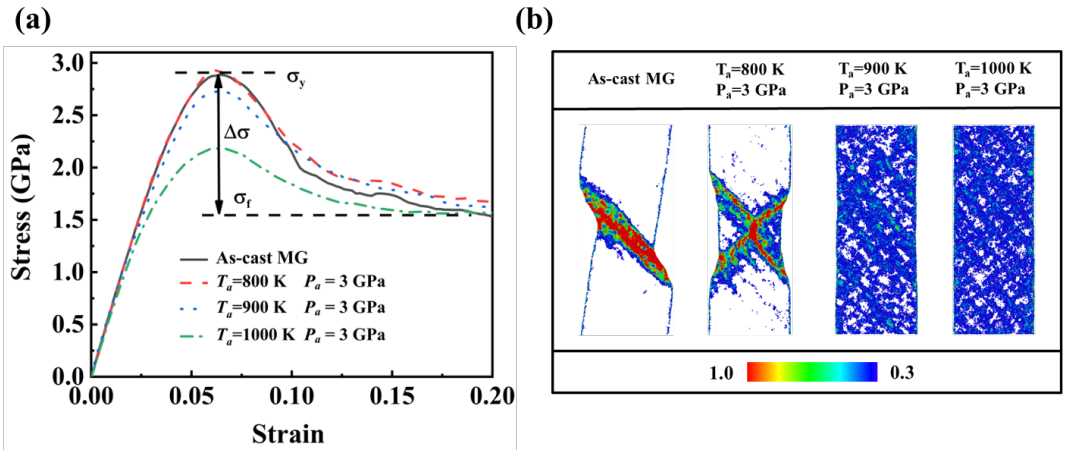

Fig. 3. (a) Uniaxial tensile stress-strain curves for the as-cast and post-processed $Cu_{64}Zr_{36}$ MGs. (b) Deformation snapshots at a 0.2 tensile strain. The color mapping represents the local shear strain.

Thermal pressure loading exerts a significant influence on stress-strain curves, particularly on the yield stress (σ_y) and flow stress (σ_f) values. The difference between σ_y and σ_f, denoted as $\Delta\sigma = \sigma_y - \sigma_f$, is used to indicate the degree of softening and reveal changes in the plastic deformation mechanism [15]. A larger $\Delta\sigma$ value corresponds to easier strain-softening. The results, listed in Table 1, demonstrate that as the annealing temperature increases, the value of $\Delta\sigma$ decreases, indicating that shear banding gradually transforms into homogeneous plastic flow.

To demonstrate the impact of thermal pressure loading on the strength of MGs, we analyzed their elastic constants. The Young's modulus *E* and shear modulus *G* are commonly used to measure the strength of MGs, with higher values indicating greater strength [25]. Fig. 4 displays the calculated values of *E* and *G* for the post-processed MGs annealed at temperatures of 800 K, 900 K, and 1000 K. The *E* values for these samples are found to be 82.05 GPa, 79.47 GPa, and 73.16 GPa, respectively, while the corresponding *G* values are 29.56 GPa, 28.53 GPa, and 26.20 GPa, respectively. As the annealing temperature increases, both *E* and *G* values decreased continuously, indicating a strength reduction. The results demonstrate that increasing the annealing temperature results in a gradual weakening of MGs.

Table 1

Summary of softening degree ($\Delta\sigma$) results after thermal pressure loading.

	As-cast MG	Post-processed MGs		
		T_a = 800 K	T_a = 900 K	T_a = 1000 K
σ_y (GPa)	2.90	2.90	2.73	2.18
$\Delta\sigma = (\sigma_y - \sigma_f)$	1.28	1.13	1.09	0.64

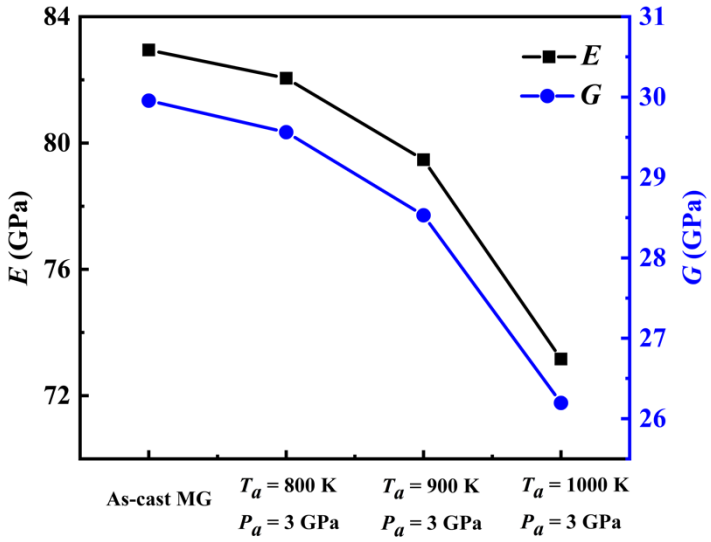

Fig. 4. Effect of thermal pressure loading on Young's modulus and shear modulus of $Cu_{64}Zr_{36}$ MGs. The black and blue lines represent the *E* and *G* values, respectively, while the symbols represent the corresponding data points.

3.2.2. Amorphous microstructures

The process of MG rejuvenation has been found to result in a fictive temperature increase, which is intimately connected with the amorphous microstructures [26]. Thus, it is of crucial to investigate the effect of rejuvenation on the microstructures of MGs. In this study, we analyzed the gradient atomic packing microstructures model to examine the structural changes caused by thermal pressure loading. This model, proposed by Luo *et al.* [27], allows for the deduction of hidden order within the amorphous microstructures based on the geometrical frustration of polyhedral, which is classified into six species represented by Roman numerals I to VI [28].

From the perspective of atomic packing, the amorphous can be divided into three regions: solid-like, transition, and liquid-like [29]. The solid-like region is responsible for the strength of the material and consists of stable motifs that are highly resistant to shear transformation. This region is primarily composed of the I polyhedral species. The liquid-like region, on the other hand, is responsible for the plasticity of the material and consists of unfavorable topological clusters that are more conducive to the initiation of shear localization. This region includes the IV, V, and VI polyhedral species. The

transition region is an intermediary between the solid-like and liquid-like regions and includes the II and III polyhedral species. Shear transformation zones (STZs) occur primarily in the liquid-like regions of the amorphous material due to its local structural heterogeneities, which then evolve into shear bands [30]. While liquid-like regions promote the nucleation of the shear band, solid-like regions impede its propagation [29].

Figure 5(a)-(c) compares the gradient atomic packing microstructures in the as-cast and post-processed MGs. The most important polyhedral for $Cu_{64}Zr_{36}$ MGs is the full icosahedra (FI) with Voronoi index <0,0,12,0>, which is the backbone microstructures of MGs and is closely related to the ordered microstructures and is depicted in Fig. 5(a). The gradient atomic packing microstructures model in Fig. 5 indicates that the fraction of polyhedral changes after thermal pressure loading. It is observed that the fraction of solid-like region and transition region increases with the increase of annealing temperature, while the fractions of liquid-like regions are gradually decreasing. This seems contradictory to the finding that the plasticity of MGs increases while the strength decreases following thermal pressure rejuvenation. However, this is mainly due to the fact that the liquid-like regions are more easily compressed to accommodate the volume reduction under compressive pressure, leading to a decrease in the fraction of liquid-like regions accompanied by an increase in the fraction of strength-related solid-like regions. Moreover, the fraction of Cu-centered <0,0,12,0> remains almost constant as the annealing temperature decreases (see Fig. 5(a)). Therefore, further investigation is required to understand the structural order in MGs.

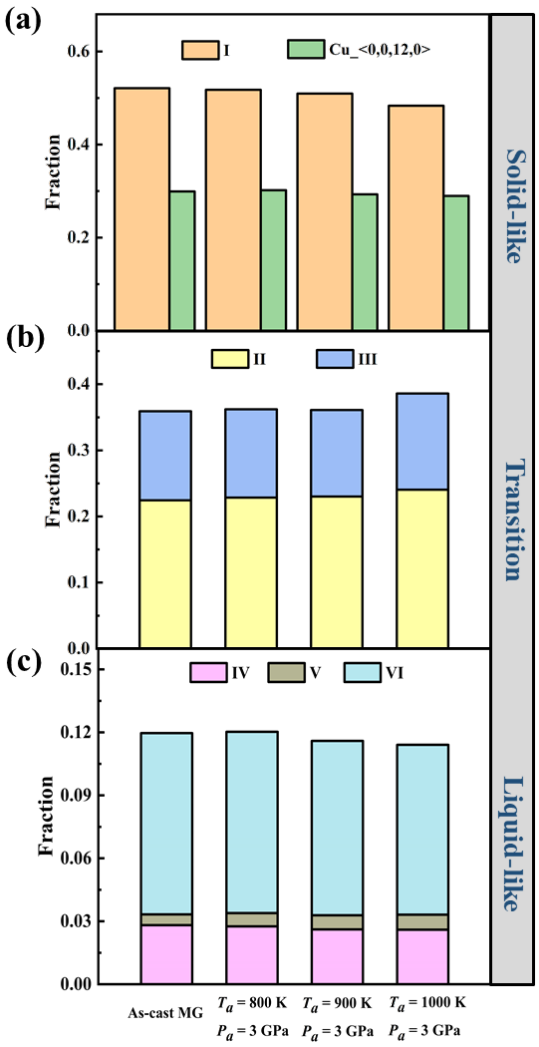

Fig. 5. Variation in the fraction of different kinds of atoms after thermal pressure loading on $Cu_{64}Zr_{36}$ MGs. (a), (b), and (c) show the fraction of solid-like, transition, and liquid-like regions in as-cast and post-processed MGs, respectively. The fraction of Cu-centered <0,0,12,0> clusters is shown in (a) for reference.

Many theoretical studies have focused solely on short-range-order (SRO) while neglecting the role of medium-range-order (MRO), which leads to inaccurate predictions of the internal structural characteristics of MGs. SRO refers to the ordered atomic polyhedra in the range of the first nearest neighbor [31], while MRO, which extends beyond the nearest-neighbor interaction, is constructed by various polyhedra packing [31, 32]. As shown in Fig. 6(a), the average and maximum size of MRO in MGs increase with increasing annealing temperature, indicating that the internal

microstructures of MGs becomes more ordered [32]. These findings highlight the importance of considering MRO when studying the microstructures of MGs. Moreover, the results in Fig. 6(a) suggest that the microstructures of MGs transforms to a high-energy ordered state after thermal pressure rejuvenation. Compressive pressure modulates the local atomic environment in $Cu_{64}Zr_{36}$ MGs by changing the average chemical composition and bond length associated with the local atomic environment [33]. As a result, the microstructures become more ordered under compressive pressure, even though the MGs become more energetic due to rejuvenation.

It is widely recognized that free volume is an inherent structural defect in MGs and plays a significant role in their deformation mechanisms [34]. The higher the free volume fraction, the more readily plastic flow occurs. However, it is challenging to measure changes in free volume because it is distributed among atoms, and it is highly sensitive to local structural configurations. To address this issue, the Voronoi volume less the atom core volume has been proposed as a means of quantifying changes in free volume [34]. The formula is given by $V_{free} = V_{voro} - V_{atom}$, where V_{voro} and V_{atom} are the Voronoi atomic volume and the atom core volume, respectively. Fig. 6(b) displays the changes in free volume of MGs following thermal pressure loading. It is evident that the fraction of free volume decreases with increasing annealing temperature. This finding contradicts a homogeneous plastic deformation mechanism and can be attributed to the effect of compressive pressure on the microstructures. These results indicate that post-processed MGs can achieve a high-energy rejuvenation state, even as the microstructures becomes more ordered and the fraction of free volume decreases.

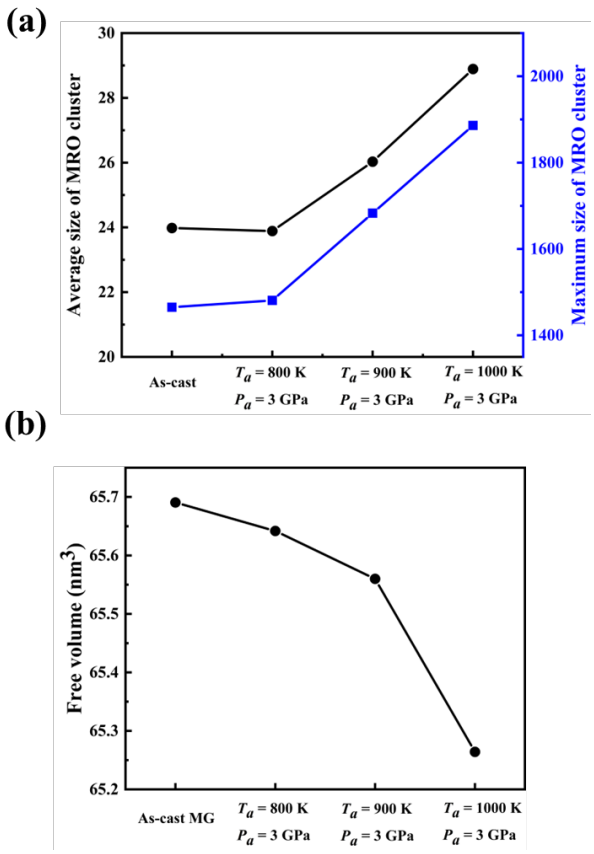

Fig. 6. Microstructures and free volume analysis of as-cast and post-processed $Cu_{64}Zr_{36}$ MG. Samples here are processed by thermal pressure loading. (a) The average and maximum sizes of MRO clusters in as-cast and post-processed MGs. (b) Free volume for the as-cast and post-processed MG samples.

3.3. Biaxial tensile loading

3.3.1. Mechanical properties

Figure 7(a) illustrates the stress-strain curves of both the as-cast and the post-processed MGs subjected to various loading stresses σ_c. In the simulations, the loading stress of the post-processed MGs ranges between 70% and 90% of the yield stress (σ_y = 2.9 GPa). As shown in Fig. 7(a), as the loading stress increases, the decrease in flow stress slows down gradually, while the yield stress of all MGs remains essentially unchanged, indicating strain delocalization. To observe the extent of delocalization in the plastic flow of MGs, we examined the deformation processes by analyzing the local shear strain. Fig. 7(b) shows a sequence of snapshots that capture the deformation in

the MGs. The as-cast MG sample exhibits catastrophic failure with shear banding. However, the post-processed MGs at loading stresses σ_c = 2.3 GPa (Fig. 7(b)) display dominant shear bands, indicating localized plastic flow. At loading stresses σ_c = 2.4 GPa, σ_c = 2.5 GPa, σ_c = 2.6 GPa, there is no evidence of shear banding, and the post-processed MGs exhibit homogeneous plastic flow. Thus, there is a transition in the deformation mode of the MGs from localized shear banding to homogeneous plastic flow as the loading stress increases.

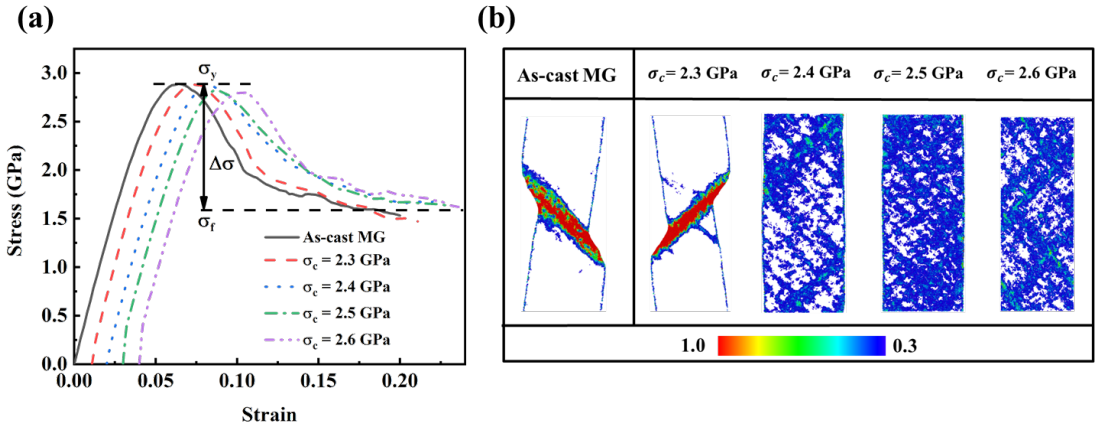

Fig. 7. Mechanical properties of as-cast and post-processed $Cu_{64}Zr_{36}$ MGs. (a) Tension stress-strain curves for as-cast and post-processed MGs and (b) snapshots of microstructures deformation at a 0.2 strain. The color map indicates the local shear strain.

Table 2 presents the calculated $\Delta\sigma$ values. At a loading stress of σ_c = 2.3 GPa, the post-processed and as-cast MGs exhibit similar $\Delta\sigma$ values, indicating that ductility is not significantly improved. As loading stress increases, the $\Delta\sigma$ of post-processed MGs gradually becomes smaller than that of as-cast MGs, suggesting that there may be no shear localization and that tensile ductility is enhanced. In contrast to Kalcher *et al.* [35], which found that 40 ns of uniaxial elastostatic tensile loading at 500 K was necessary to improve the plasticity of $Cu_{64}Zr_{36}$ MGs, these results show that biaxial tensile loading at room temperature can rejuvenate $Cu_{64}Zr_{36}$ MGs in just 20 ns. Table 2 also shows that the yield stress of post-processed MGs is not lower than 2.8 GPa. After biaxial tensile loading, the yield stress decreased by no more than 2.8%, which is a significant

improvement over Kalcher *et al.* [35]. Previous studies have shown that uniaxial loading stresses near the yield stress can cause localized shear banding [21]. However, our simulations demonstrate that biaxial tensile loading not only does not induce shear banding at loading stresses close to the yield stress but is also more effective in improving toughness compared to uniaxial tensile loading.

Table 2

Summary of softening degree ($\Delta\sigma$) results for $Cu_{64}Zr_{36}$ MG.

	As-cast MG	Post-processed MGs			
		σ_c= 2.3 GPa	σ_c= 2.4 GPa	σ_c= 2.5 GPa	σ_c= 2.6 GPa
σ_y (GPa)	2.90	2.88	2.87	2.82	2.80
σ_c /σ_y	/	79%	83%	86%	90%
$\Delta\sigma = (\sigma_y - \sigma_f)$	1.28	1.26	1.14	1.11	1.05

The transition in the deformation mode observed can be explained by the larger residual shear strain in the post-processed MGs sample resulting from biaxial tensile loading. To quantify the fraction of atoms retaining larger shear strain, we use the von Mises strain $\eta^{Mises} = \sqrt{\frac{1}{2}Tr(\eta - \eta_m I)^2}$, which is defined as the square root of half the trace of the deviatoric strain tensor, η, minus the local hydrostatic strain, η_m, of an atom [36, 37]. In this work, we consider atoms with a η^{Mises} greater than 0.3 as S-atoms. A region with several tens or hundreds of S-atoms is more susceptible to evolve into a STZ. The accumulation of STZs generates a shear band that propagates rapidly due to the absence of defects in MGs that can prevent it, ultimately leading to failure [38]. Indeed, due to the local structural heterogeneities of MGs, STZs are primarily concentrated in the local region when stress is imposed [39]. Nevertheless, increasing the fraction of S-atoms can promote the homogeneous distribution of STZs in MGs, ensuring delocalized plastic flow.

In Fig. 8, we can observe the fraction of S-atoms for post-processed MGs. At a loading stress of σ_c = 2.3 GPa, the fraction of S-atoms is low, which causes the STZ to accumulate in local areas leading to catastrophic failure of the MGs. However, with the increase in loading stress (σ_c = 2.4 GPa, σ_c = 2.5 GPa, and σ_c = 2.6 GPa), the fraction of S-atoms increases. After tension to a strain of 0.2, the MGs exhibit no evidence of shear banding, indicating enhanced tensile ductility and prevention of catastrophic failure. This is attributed to the uniformly distributed STZ in the MGs, which is generated by the accumulation of S-atoms and ultimately rejuvenates the MGs.

The above results suggest that a stress level above 80% of the yield stress is necessary for achieving uniform distribution of STZs through biaxial tensile loading at room temperature. Any stress level below this threshold may not be effective in improving the plasticity of the material. Therefore, our findings in Fig. 7 and Fig. 8 emphasize the importance of identifying the appropriate stress threshold for achieving the desired mechanical properties through biaxial tensile loading.

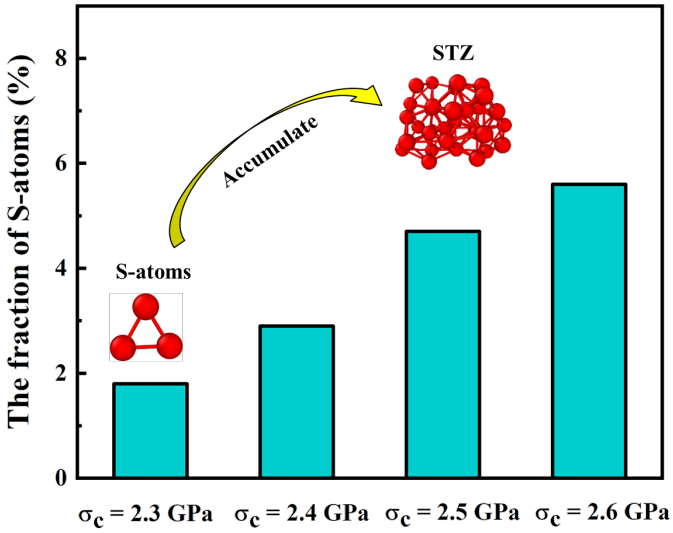

Fig. 8. Evolution of S-atoms into a STZ in post-processed MGs. The main plot shows the fraction of S-atoms at different pressure values, while the inset illustrates the process of S-atoms evolving into an STZ.

Figure 9 illustrates the calculated values of Young's modulus *E* and shear modulus *G* for the post-processed MGs under different loading stresses. The results demonstrate a continuous decrease in both *E* and *G* with the increase in loading stress, indicating a

reduction in strength. At 2.3, 2.4, 2.5, and 2.6 GPa loading stresses, the values of *E* for the post-processed MGs are 82.64, 82.09, 81.93, and 81.12 GPa, respectively. The corresponding *G* values are 29.76, 29.5, 29.49, and 29.15 GPa, respectively. However, the decrease in Young's modulus is within 2.1%, and the drop in shear modulus is within 2.7%. These findings suggest that biaxial tensile loading effectively enhances the plasticity of MGs without compromising too much strength.

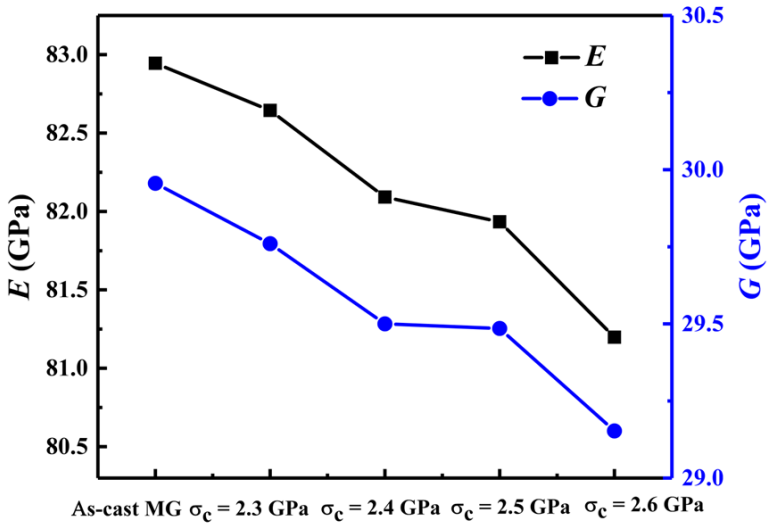

Fig. 9. Effect of biaxial tensile loading on Young's modulus and shear modulus of $Cu_{64}Zr_{36}$ MGs.

3.3.2. Irreversible deformation induced by biaxial loading

Previous experimental studies [21, 40, 41] and simulation [35] have demonstrated that permanent deformation of MGs in the elastostatic regime can be achieved by removing the applied stress. This permanent deformation does not occur abruptly upon the application of stress, but rather is induced by prolonged stress loading, with the degree of deformation being influenced by the loading stress [35]. These findings suggest that irreversible structural changes may occur in the elastostatic regime, leading to permanent deformation [21, 40]. Fig. 10(a) displays the equivalent strain and time curves of MGs subjected to biaxial tensile loading at room temperature. The equivalent strain is defined as [42]:

$$\varepsilon_e = \sqrt{\frac{2}{9}\left[\left(\varepsilon_x - \varepsilon_y\right)^2 + \left(\varepsilon_y - \varepsilon_z\right)^2 + (\varepsilon_x - \varepsilon_z)^2 + 6\left(\gamma_{xy}^2 + \gamma_{xz}^2 + \gamma_{yz}^2\right)\right]} \quad (1)$$

where ε_x, ε_y, and ε_z are principal strain in the direction of *x*, *y*, and *z*, respectively; γ_{xy}, γ_{xz}, and γ_{yz} are shear strain in the direction of *xy*, *xz*, and *yz*, respectively. During the loading-unloading process, the shear strains all equal zero, i.e., $\gamma_{xy} = \gamma_{xz} = \gamma_{yz} = 0$. The equivalent strain of the MGs is comprised of three components: elastic response (ε_E), anelastic response (ε_A), and viscoelastic response (ε_V). When the loading stress is removed from the MGs, the elastic and anelastic strains can recover, while the viscoelastic strains cannot (see Fig. 10(a)). This indicates that the MGs undergo permanent deformation during the elastic loading. The biaxial tensile loading at room temperature causes a permanent structural change in the MGs, leading to a modification of their mechanical properties.

Figure 10(b) illustrates the equivalent strain versus time during relaxation under various loading stresses, consisting of both primary and secondary stages. In the primary stage, the displacement increases markedly with time and then becomes smoother in the secondary stage. To represent the deformation rate, we use the slope within the time interval between *t* = 5 ns and *t* = 20 ns [35]. The deformation rate values calculated for MGs are 0.0138 (σ_c = 2.3 GPa), 0.0176 (σ_c = 2.4 GPa), 0.0349 (σ_c = 2.5 GPa), and 0.0508 (σ_c = 2.6 GPa), respectively. During the relaxation process, MGs with loading stress of σ_c = 2.3 GPa exhibit a relatively slow deformation rate, while the rate of deformation increases significantly with increasing loading stress. When the loading stress is below 80% of the yield stress (e.g., σ_c = 2.3 GPa), the increase in displacement is insufficient to affect the microstructures of the MGs. However, when the loading stress exceeds 80% of the yield stress, the MGs exhibit a greater deformation rate, indicating a more significant structural change. As the loading stress increases, the deformation rate also increases because the proportion of viscoelastic strain becomes larger. Thus, a higher deformation rate implies a greater degree of structural change [35].

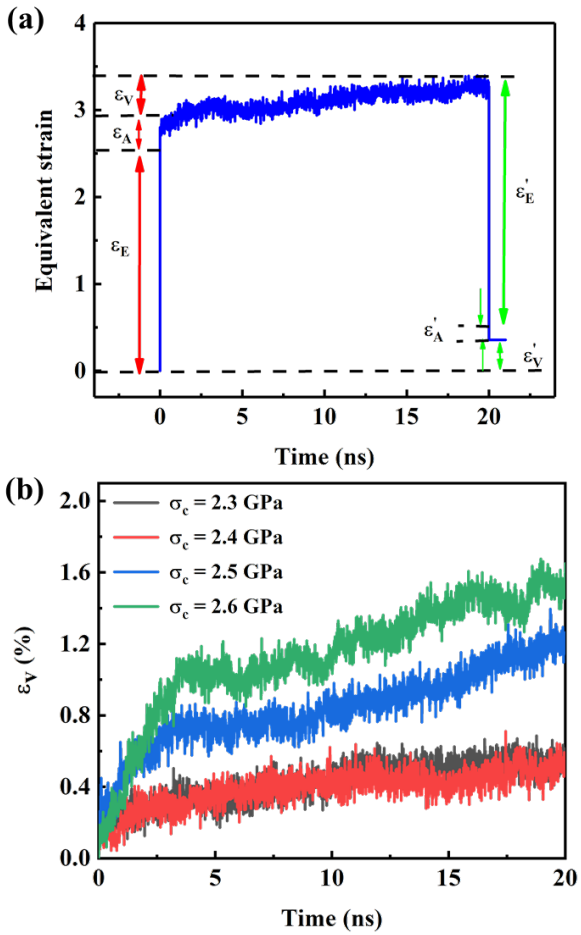

Fig. 10. Equivalent strain response of post-processed MG under different loading stresses. (a) Equivalent strain vs. time curves for post-processed MG under loading stress. (b) Equivalent strain vs. time at various loading stresses. The ε_E, ε_A, and ε_V are the strain components corresponding to the elastic responses, anelastic responses, and viscoelastic responses during the loading stage, whereas ε'_E, ε'_A, and ε'_V are the same components measured during the unloading stage.

Moderate biaxial tensile loading is beneficial for MGs since it can restore the macroscopic plasticity lost due to annealing. However, for MGs with loading stress σ_c = 2.3 GPa, the same loading time does not alter their mechanical properties because the structural change is insufficient. When the loading stress exceeds 80% of the yield stress, room temperature biaxial tensile loading has a positive effect on the mechanical properties of MGs. The findings in Fig. 10(a) and (b) highlight that permanent deformation in the elastic regime leads to a change in the amorphous microstructures,

which affects the transition of the plastic deformation mechanism from brittle to ductile.

3.3.3. Amorphous microstructures

Inducing structural disordering through permanent deformation of MGs in the elastic regime can significantly alter their mechanical properties [40]. The changes in the fraction of polyhedral after biaxial tensile loading are shown in Fig. 11(a)-(c). For post-processed MGs with loading stress of σ_c = 2.3 GPa, the fraction of the liquid-like region increases slightly, while that of the solid-like region remains nearly unchanged. Consequently, the mechanical properties of MGs with stress σ_c = 2.3 GPa do not change significantly. However, for post-processed MGs with loading stress of σ_c = 2.4 GPa and σ_c = 2.5 GPa, the fraction of the solid-like region remains almost constant, while the fraction of the liquid-like region increases, leading to MGs with strong and tough mechanical properties. In contrast, for post-processed MGs with a loading stress of σ_c = 2.6 GPa, the fraction of the solid-like region decreases slightly, while the fraction of the liquid-like region increases significantly. This result is consistent with the previous observations of stronger-and-tougher MGs after biaxial tensile loading. Moreover, as shown in Fig. 11(a), when the loading stress is σ_c = 2.4 GPa, σ_c = 2.5 GPa, and σ_c = 2.6 GPa, the post-processed MGs exhibit a lower fraction of FI, indicating a more disordered microstructures.

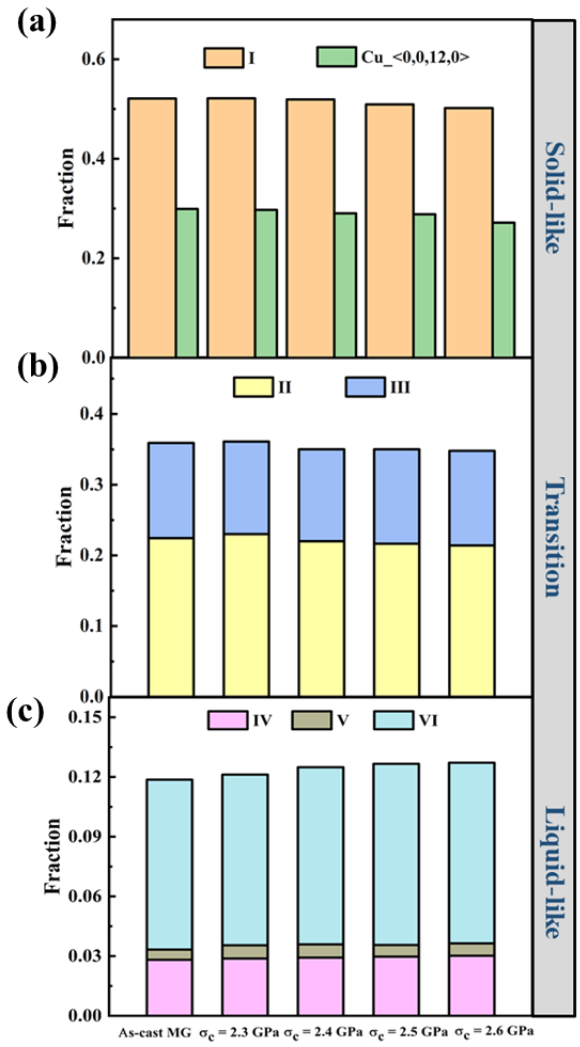

Fig. 11. Variation in the fraction of different kinds of atoms after biaxial tensile loading. (a), (b) and (c) show the fraction of the solid-like, transition, and liquid-like regions in as-cast and post-processed MGs, respectively. The fraction of Cu-centered <0,0,12,0> is shown in (a) as a reference.

The results shown in Fig. 12(a) and (b) suggest that biaxial tensile loading induces structural disordering in MGs, resulting in a decrease in the average and maximum size of the MRO clusters and an increase in the free volume. The decrease in the size of the MRO clusters indicates that the internal microstructures of MGs becomes more disordered, which is consistent with the observations in Fig. 11(a)-(c). The increase in free volume suggests that biaxial tensile loading is beneficial to plastic flow, as there is more space for atomic rearrangement during plastic deformation. Overall, these results

indicate that biaxial tensile loading can induce structural disordering in MGs, leading to stronger and tougher mechanical properties.

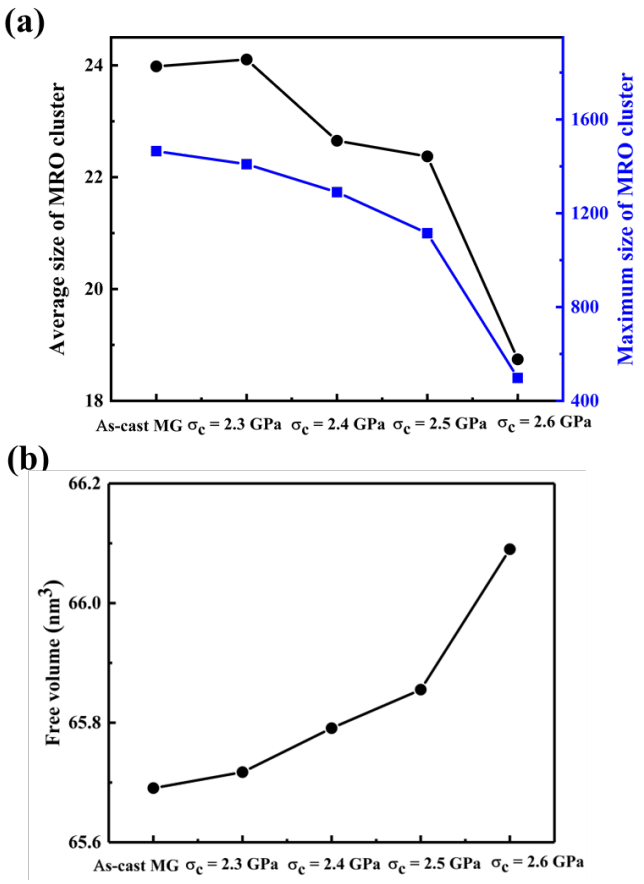

Fig. 12. Microstructures and free volume analysis of as-cast and post-processed $Cu_{64}Zr_{36}$ MGs. (a) Samples here are processed by biaxial tensile loading. The average and maximum sizes of MRO clusters in as-cast and post-processed MGs. (b) Free volume for the as-cast and post-processed MG samples.

3.3.5. The average degree of the five-fold local symmetry

To reveal the changes in the microstructures during the tension, we use the average degree of the five-fold local symmetry $W = \sum_i (f_i^5 \times P_i)$, where f_i^5 is the fraction of pentagonal in Voronoi polyhedron type i, which is defined as $f_i^5 = n_i^5 / \sum_{k=3,4,5,6} n_i^k$, n_i^k is the number of k-edged polygon in Voronoi polyhedron type i, P_i is the fraction of polyhedron type i [43].

In $Cu_{64}Zr_{36}$ MGs, the regions with lower degree of five-fold symmetry, referred to

as liquid-like regions, have higher potential energy, lower packing density, and an unstable configuration state. Plastic deformation occurs more easily in these regions [44]. However, further plastic deformation can only occur in regions with higher degree of five-fold symmetry, as regions with lower degree of five-fold symmetry cannot accommodate more plastic strains [44]. Typically, geometrically unfavorable motifs, such as liquid-like regions, have a lower degree of five-fold symmetry, while solid-like regions have a higher degree of five-fold symmetry [45, 46].

The variation of the W parameter with tension strain in the MG samples is shown in Fig. 13. It is apparent that both the as-cast and the post-processed MG with a critical stress of σ_c = 2.3 GPa exhibit comparable behavior. Specifically, a rapid decrease in W occurs above ε = 0.1, followed by reaching constant values below ε = 0.1. This drop in W is attributed to the breaking of clusters in solid-like regions and their transformation into clusters in liquid-like regions. The constant W is primarily due to the formation of a shear band, which ultimately leads to the catastrophic fracture of the MGs. For loading stresses σ_c > 80% (e.g., σ_c = 2.4 GPa, σ_c = 2.5 GPa, σ_c = 2.6 GPa), the W value continues to decrease until the tension reaches ε = 0.2. Consequently, the shift in the deformation mechanism of post-processed MGs from shear banding to homogeneous plastic deformation can be attributed to the changes in W.

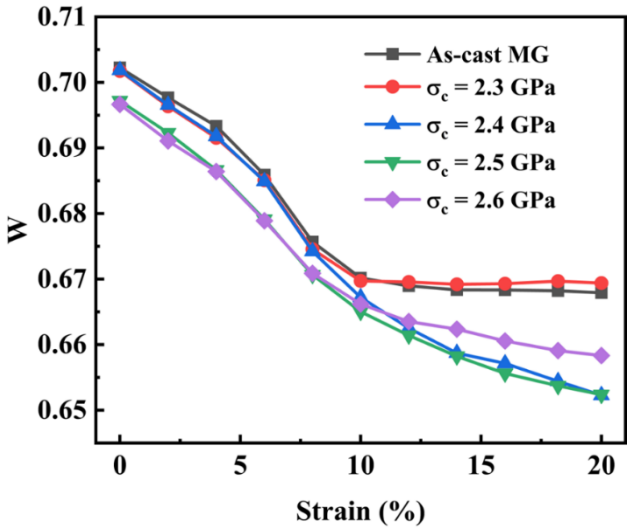

Fig. 13. The evolution of the average degree of the five-fold local symmetry W during tension.

3.4. Cryogenic thermal cycling

3.4.1. Mechanical properties

The stress-strain curves of as-cast and post-processed MGs with different cycle numbers are illustrated in Fig. 14(a). The MGs were subjected to uniaxial tensile loading at cycle numbers of 15, 20, 25, 30, and 35. The value of ΔE tends to stabilize after the 20th cycle. Therefore, we compared the tensile behavior of the MGs prior to and after stabilization of ΔE. It was observed that at the 15th cycle, the flow stress slightly increased, while the yield stress remained essentially unchanged. These results suggest that the deformation mechanism of MGs did not change significantly. However, for cycle numbers between 20 and 35, the yield stress decreased significantly while the flow stress showed minor changes, indicating a change in the deformation mechanism of $Cu_{64}Zr_{36}$ MG. Fig. 14(b) presents a sequence of snapshots capturing the structural deformation in MGs. When the cycle number is 15, primary and secondary shear bands appear, leading to localized plastic flow. Conversely, for cycle numbers between 20 and 35, there is no mature shear band in the $Cu_{64}Zr_{36}$ MG, suggesting that the material has good ductility.

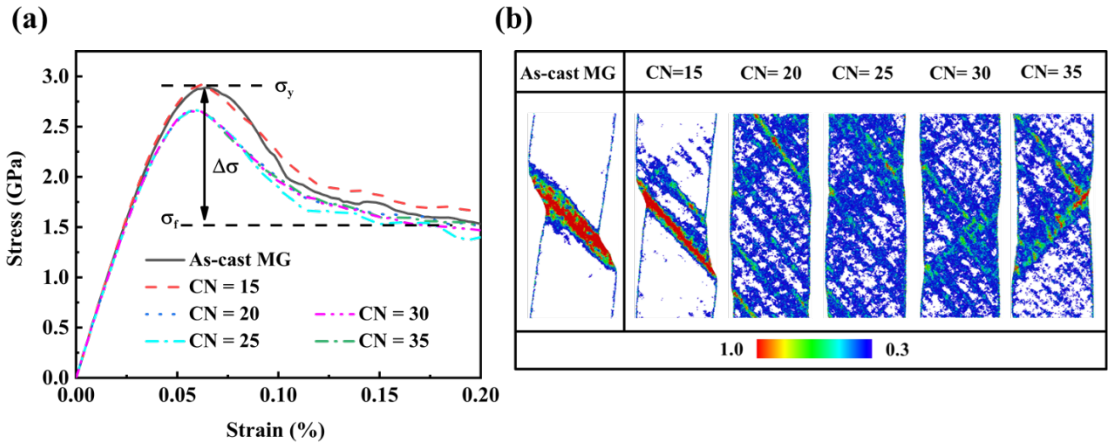

Fig. 14. (a) Tension stress-strain curves for as-cast and post-processed MGs. (b) Snapshots of microstructures deformation at a 0.2 strain. The color indicates the local shear strain.

To investigate the change in plastic flow, we calculated $\Delta\sigma$, and the results are presented in Table 3. The values of $\Delta\sigma$ gradually decrease as the cycle number increases

and become stable. Therefore, the change in the plasticity mechanism of MGs with the cycle number can be divided into two parts: first, the plastic flow improves as the cycle number increases; second, the plastic flow does not change significantly as the cycle number continues to increase. The findings in Fig. 14 and Table 3 demonstrate that increasing the cycle number above 20 enhances the plasticity of $u_{64}Zr_{36}$ MG. However, it is essential to note that the improvement in plasticity does not change significantly with the continuous increase in the cycle number.

Table 3

Summary of softening degree ($\Delta\sigma$) results of $Cu_{64}Zr_{36}$ MG.

	As-cast	Post-processed MGs				
	MG	CN = 15	CN = 20	CN = 25	CN = 30	CN = 35
σ_y (GPa)	2.90	2.91	2.66	2.66	2.65	2.66
$\Delta\sigma = (\sigma_y - \sigma_f)$	1.28	1.22	1.06	1.04	1.08	1.11

Figure 15 illustrates that the values of Young's modulus *E* and shear modulus *G* for $Cu_{64}Zr_{36}$ MG decrease after cryogenic thermal cycling, suggesting a decrease in the material's strength. The values of *E* for the post-processed MGs at cycle numbers of 15, 20, 25, 30, and 35 are 81.73, 80.12, 79.46, 80.11, and 80.28 GPa, respectively. Correspondingly, the *G* values are 29.45, 28.36, 27.92, 28.22, and 28.39 GPa, respectively. When the number of cycles is greater than 20, the values of *E* and *G* tend to stabilize, suggesting that the strength change of MGs is stable. This observation is consistent with the above-mentioned findings of changes in stress-strain.

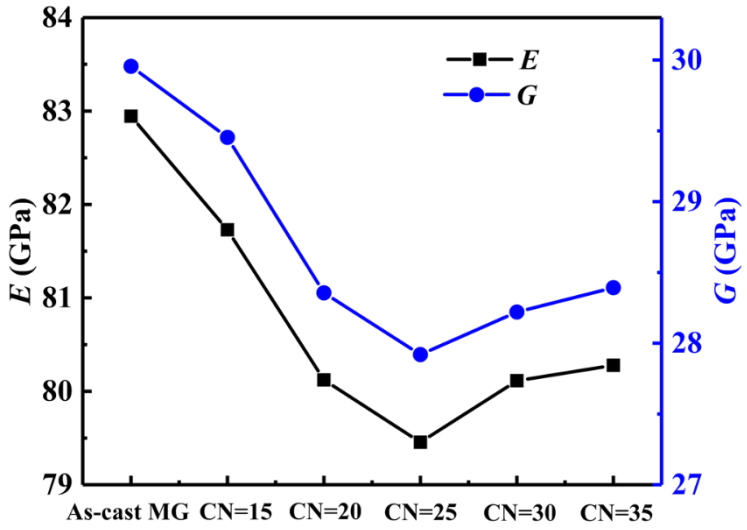

Fig. 15. Effect of cryogenic thermal cycling on Young's modulus and shear modulus of $Cu_{64}Zr_{36}$ MGs.

3.4.2. Amorphous microstructures

Figure 16(a)-(c) shows the change in the fraction of polyhedral after cryogenic thermal cycling. The fraction of solid-like regions remained stable when the cycle number was increased to 15, indicating no significant decrease in the strength of the MGs. However, when the cycle number increased to between 20 and 35, the fraction of solid-like regions decreased, suggesting a reduction in the strength of the MGs. Moreover, in this cycle range, the fraction of <0,0,12,0> also decreased, indicating a more disordered microstructures of the MGs. The polyhedral fraction in the transition region remained roughly constant after cryogenic thermal cycling. Notably, when the cycle number was between 20 and 35, the fraction of polyhedral in the liquid-like region increased significantly, suggesting a possible improvement in the ductility of MGs. Overall, the results demonstrate an increase in the ductility and a decrease in the strength of MGs after cryogenic thermal cycling. In addition, the factors affecting the number of atoms in the liquid-like region are different for different rejuvenation modes. In the present work, the number of atoms in the liquid-like region does not vary much, which is possibly related to the chosen parameters.

In comparison with cryogenic thermal cycling and biaxial loading, the solid-like region and liquid-like region exhibit completely different changes after thermal

pressure loading, which is mainly attributed to the compressive pressure during thermal pressure loading. The liquid-like region is more prone to be squeezed and the reduction in volume at high pressure, while the solid-like region associated with dense packing increases. One possible reason for the failure to find a correlation between the reduction of liquid-like region and the enhanced plasticity is that rejuvenation is associated with an increase in the fictive temperature [26].

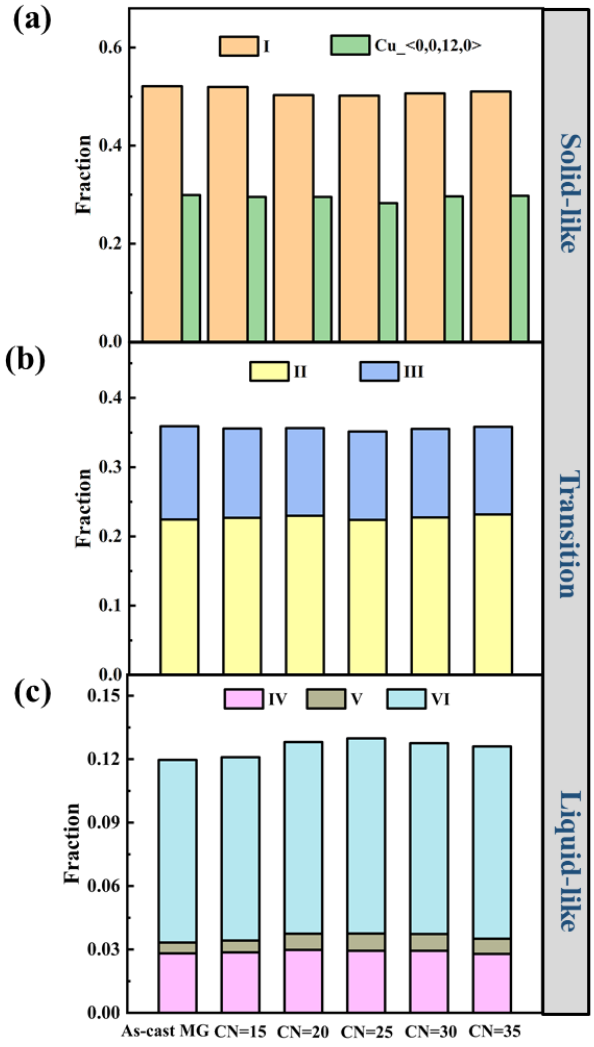

Fig. 16. Variation in the fraction of different kinds of atoms after cryogenic thermal cycling. (a), (b) and (c) show the fraction of the solid-like, transition, and liquid-like regions in as-cast and post-processed MGs, respectively. The fraction of Cu-centered <0,0,12,0> is shown in the (a).

The changes in the average and maximum size of the MRO clusters of $Cu_{64}Zr_{36}$

MG after cryogenic thermal cycling are presented in Fig. 17(a). It is observed that both the average and maximum size of MRO clusters decrease after thermal cycling. Furthermore, when the cycle number exceeds 20, the average and maximum sizes of MRO clusters decrease significantly, indicating a more disordered internal microstructures of $Cu_{64}Zr_{36}$ MG. This disordered microstructure promotes homogeneous plastic flow, but it also leads to a breakdown of the rigid backbone microstructures, causing a decrease in strength.

Figure 17(b) illustrates the impact of cryogenic thermal cycling on the fraction of free volume in $Cu_{64}Zr_{36}$ MG. The results show that the fraction of free volume increases with the cycle number, and when the cycle number exceeds 20, the increased free volume tends to stabilize. At this stage, the ductility of the MGs is found to have improved significantly due to the presence of increased free volume. In contrast, when the cycle number is too small, such as 15 cycles, the free volume increases less and does not significantly affect the ductility of $Cu_{64}Zr_{36}$ MG. Therefore, it can be concluded that cryogenic thermal cycling significantly increases the fraction of free volume in $Cu_{64}Zr_{36}$ MG, which eventually improves its room temperature plasticity, especially when the cycle number is sufficient.

The results in Fig. 17 emphasize that the $Cu_{64}Zr_{36}$ MG evolves into a high-energy disordered structural state after cryogenic thermal cycling. The free volume of MGs increases after cryogenic thermal cycling, which provides an excellent condition for homogeneous plastic flow.

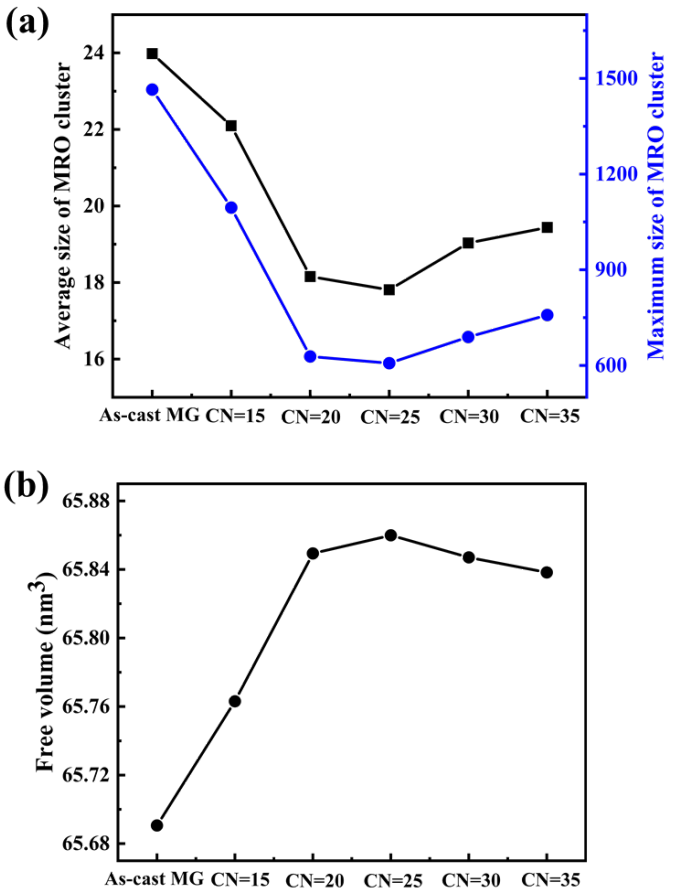

Fig. 17. Microstructures and free volume analysis of as-cast and post-processed $Cu_{64}Zr_{36}$ MGs. (a) Samples here are processed by cryogenic thermal cycling. The average and maximum sizes of MRO clusters in as-cast and post-processed MGs. (b) Free volume for the as-cast and post-processed MG samples.

4. Conclusions

In conclusion, this study investigates the effects of various MG rejuvenation modes using MD simulations. The results show that biaxial tensile loading is a feasible rejuvenation method for $Cu_{64}Zr_{36}$ MGs and that it is more effective in toughening than uniaxial tensile loading. The rejuvenation of MGs through thermal pressure loading results in the highest plastic performance, while biaxial tensile loading can achieve the highest strength. Cryogenic thermal cycling can also rejuvenate MGs, to be noted, with less sacrifice in strength than thermal pressure loading. The microstructures of the rejuvenated MGs processed by the different methods are characterized by high-energy ordered or disordered glass states. These findings not only contribute to our

understanding of the effect of rejuvenation modes on the structure and mechanical properties of MGs, but also provide valuable guidance for developing stronger and tougher MGs for practical applications in the fields automotive components, medical devices, and aerospace parts.

CRediT authorship contribution statement

Shan Li: Data curation, Analyses data, Writing-original draft. **Yue Yu:** Investigation. **Paulo S. Branicio:** Supervision, Visualization. **Zhen-Dong Sha:** Funding acquisition, Supervision, Analyses data, Conceived and directed the work.

Declaration of competing interest

The authors declare that they have no known competing financial interests or personal relationships that could have appeared to influence the work reported in this paper.

Acknowledgments

SL and ZDS would like to acknowledge the financial support by the National Natural Science Foundation of China, through grant no. 11972278. ZDS is also grateful for the support from Opening fund of State Key Laboratory of Nonlinear Mechanics. PSB acknowledge financial support by the US Department of Energy, Office of Science, Office of Basic Energy Sciences, under Award Number DE-SC0020295.

References

[1] W.H. Wang, Dynamic relaxations and relaxation-property relationships in metallic glasses, Prog. Mater. Sci. 106 (2019) 100561.

[2] F. Meng, K. Tsuchiya, I. Seiichiro, Y. Yokoyama, Reversible transition of deformation mode by structural rejuvenation and relaxation in bulk metallic glass, Appl. Phys. Lett. 101(12) (2012) 121914.

[3] C. Ebner, S. Pauly, J. Eckert, C. Rentenberger, Effect of mechanically induced

structural rejuvenation on the deformation behaviour of CuZr based bulk metallic glass, Mater. Sci. Eng.A 773 (2020) 138848.

[4] L. Zhao, K.C. Chan, S.H. Chen, S.D. Feng, D.X. Han, G. Wang, Tunable tensile ductility of metallic glasses with partially rejuvenated amorphous structures, Acta Mater. 169 (2019) 122-134.

[5] Y. Sun, A. Concustell, A.L. Greer, Thermomechanical processing of metallic glasses: extending the range of the glassy state, Nat. Rev. Mater. 1(9) (2016) 16039.

[6] Y. Zhang, J. Li, H. Zhou, Y. Hu, S. Ding, R. Xia, Cold welding behavior of metallic glass nanowires: Insights from large-scale numerical simulations, J. Mater. Sci. 56(28) (2021) 15906-15920.

[7] Y. Zhang, J. Li, Y. Hu, S. Ding, F. Du, R. Xia, Characterization of the deformation behaviors under uniaxial stress for bicontinuous nanoporous amorphous alloys, Phys. Chem. Chem. Phys. 24(2) (2022) 1099-1112.

[8] K. Avchaciov, Y. Ritter, F. Djurabekova, K. Nordlund, K. Albe, Controlled softening of Cu64Zr36 metallic glass by ion irradiation, Appl. Phys. Lett. 102(18) (2013) 181910.

[9] M. Wakeda, J. Saida, J. Li, S. Ogata, Controlled Rejuvenation of Amorphous Metals with Thermal Processing, Sci. Rep. 5 (2015) 10545.

[10] S. Sohrabi, M.C. Ri, H.Y. Jiang, L. Gu, P. Wen, Y.H. Sun, W.H. Wang, Prominent role of chemical heterogeneity on cryogenic rejuvenation and thermomechanical properties of La–Al–Ni metallic glass, Intermetallics 111 (2019) 106497.

[11] A. Concustell, F. Méar, S. Surinach, M. Baró, A. Greer, Structural relaxation and rejuvenation in a metallic glass induced by shot-peening, Philos. Mag. Lett. 89(12) (2009) 831-840.

[12] S. Takayama, Drawing of Pd77.5Cu6Si16.5 metallic glass wires, Mater. Sci. Eng. 38(1) (1979) 41-48.

[13] K.W. Park, C.M. Lee, M. Wakeda, Y. Shibutani, M.L. Falk, J.C. Lee, Elastostatically induced structural disordering in amorphous alloys, Acta Mater. 56(19) (2008) 5440-5450.

[14] Y. Tong, W. Dmowski, H. Bei, Y. Yokoyama, T. Egami, Mechanical rejuvenation in bulk metallic glass induced by thermo-mechanical creep, Acta Mater. 148 (2018) 384-390.

[15] S. Li, J.C. Zhang, Z.D. Sha, Mechanical behavior of metallic glasses with pressure-promoted thermal rejuvenation, J. Alloys Compd. 848 (2020) 156597.

[16] C. Wang, Z.Z. Yang, T. Ma, Y.T. Sun, Y.Y. Yin, Y. Gong, L. Gu, P. Wen, P.W. Zhu, Y.W. Long, X.H. Yu, C.Q. Jin, W.H. Wang, H.Y. Bai, High stored energy of metallic glasses induced by high pressure, Appl. Phys. Lett. 110 (2017) 111901.

[17] N. Miyazaki, M. Wakeda, Y.J. Wang, S. Ogata, Prediction of pressure-promoted thermal rejuvenation in metallic glasses, npj Comput. Mater. 2 (2016) 16013.

[18] S.V. Ketov, Y.H. Sun, S. Nachum, Z. Lu, A. Checchi, A.R. Beraldin, H.Y. Bai, W.H. Wang, D.V. Louzguine-Luzgin, M.A. Carpenter, A.L. Greer, Rejuvenation of metallic glasses by non-affine thermal strain, Nature 524 (2015) 200-203.

[19] S. Plimpton, Fast parallel algorithms for short-range molecular dynamics, J. Comput. Phys. 117 (1995) 1-19.

[20] Y.Q. Cheng, A.J. Cao, H.W. Sheng, E. Ma, Local order influences initiation of plastic flow in metallic glass: Effects of alloy composition and sample cooling history, Acta Mater. 56 (2008) 5263-5275.

[21] H.B. Ke, P. Wen, H.L. Peng, W.H. Wang, A.L. Greer, Homogeneous deformation of metallic glass at room temperature reveals large dilatation, Scr. Mater. 64(10) (2011) 966-969.

[22] B.S. Shang, W.H. Wang, A.L. Greer, P. Guan, Atomistic modelling of thermal-cycling rejuvenation in metallic glasses, Acta Mater. 213 (2021) 116952.

[23] S.V. Ketov, A.S. Trifonov, Y.P. Ivanov, A.Y. Churyumov, A.V. Lubenchenko, A.A. Batrakov, J. Jiang, D.V. Louzguine-Luzgin, J. Eckert, J. Orava, On cryothermal cycling as a method for inducing structural changes in metallic glasses, NPG Asia Mater. 10 (2018) 137-145.

[24] S.H. Chen, T. Li, W.J. Chang, H.D. Yang, J.C. Zhang, H.H. Tang, S.D. Feng, F.F. Wu, Y.C. Wu, On the formation of shear bands in a metallic glass under tailored

complex stress fields, J. Mater. Science Technol. 53 (2020) 112-117.

[25] W.H. Wang, The elastic properties, elastic models and elastic perspectives of metallic glasses, Prog. Mater. Sci. 57(3) (2012) 487-488.

[26] G. Kumar, P. Neibecker, Y.H. Liu, J. Schroers, Critical fictive temperature for plasticity in metallic glasses, Nat. Commun. 4(1) (2013) 1536.

[27] L.S. Luo, B.B. Wang, F.Y. Dong, Y.Q. Su, E.Y. Guo, Y.J. Xu, M.Y. Wang, L. Wang, J.X. Yu, R.O. Ritchie, J.J. Guo, H.Z. Fu, Structural origins for the generation of strength, ductility and toughness in bulk-metallic glasses using hydrogen microalloying, Acta Mater. 171 (2019) 216-230.

[28] B. Wang, L. Luo, E. Guo, Y. Su, M. Wang, O. Ritchie Robert, F. Dong, L. Wang, J. Guo, H. Fu, Nanometer-scale gradient atomic packing structure surrounding soft spots in metallic glasses, npj Comput. Mater. 4(1) (2020) 53-64.

[29] J. Ding, Y.Q. Cheng, E. Ma, Full icosahedra dominate local order in Cu64Zr34 metallic glass and supercooled liquid, Acta Mater. 69 (2014) 343-354.

[30] Z.D. Sha, Y. Teng, L.H. Poh, T. Wang, H. Gao, Shear Band Control for Improved Strength-Ductility Synergy in Metallic Glasses, Appl. Mech. Rev. 74(5) (2022) 050801.

[31] M. Wakeda, Y. Shibutani, Icosahedral clustering with medium-range order and local elastic properties of amorphous metals, Acta Mater. 58(11) (2010) 3963-3969.

[32] M. Lee, C.M. Lee, K.R. Lee, E. Ma, J.C. Lee, Networked interpenetrating connections of icosahedra Effects on shear transformations in metallic glass, Acta Mater. 59(1) (2011) 159-170.

[33] J. Ding, M. Asta, R.O. Ritchie, Anomalous structure-property relationships in metallic glasses through pressure-mediated glass formation, Phys. Rev. B 93(14) (2016) 140204.

[34] Q.K. Li, M. Li, Free volume evolution in metallic glasses subjected to mechanical deformation, Mater. Trans. 48(7) (2007) 1816-1821.

[35] C. Kalcher, T. Brink, J. Rohrer, A. Stukowski, K. Albe, Interface-controlled creep in metallic glass composites, Acta Mater. 141 (2017) 251-260.

[36] D. Sopu, Y. Ritter, H. Gleiter, K. Albe, Deformation behavior of bulk and nanostructured metallic glasses studied via molecular dynamics simulations, Phys. Rev. B 83(10) (2011) 100202.

[37] Y.Q. Cheng, A.J. Cao, E. Ma, Correlation between the elastic modulus and the intrinsic plastic behavior of metallic glasses: The roles of atomic configuration and alloy composition, Acta Mater. 57(11) (2009) 3253-3267.

[38] F. Shimizu, S. Ogata, J. Li, Theory of shear banding in metallic glasses and molecular dynamics calculations, Mater. Trans. 48(11) (2007) 2923-2927.

[39] E. Ma, J. Ding, Tailoring structural inhomogeneities in metallic glasses to enable tensile ductility at room temperature, Mater. Today 19 (2016) 568-579.

[40] K.W. Park, C.M. Lee, M. Wakeda, Y. Shibutani, M.L. Falk, J.C. Lee, Elastostatically induced structural disordering in amorphous alloys, Acta Mater. 56(19) (2008) 5440-5450.

[41] Y. Tong, W. Dmowski, Y. Yokoyama, G. Wang, P.K. Liaw, T. Egami, Recovering compressive plasticity of bulk metallic glasses by high-temperature creep, Scr. Mater. 69(8) (2013) 570-573.

[42] H. Ford, J.M. Alexander, Advanced Mechanics of Materials, (1963).

[43] M.Z. Li, Correlation Between Local Atomic Symmetry and Mechanical Properties in Metallic Glasses, J. Mater. Sci. Technol. 30(6) (2014) 551-559.

[44] Y.C. Hu, F.X. Li, M.Z. Li, H.Y. Bai, W.H. Wang, Five-fold symmetry as indicator of dynamic arrest in metallic glass-forming liquids, Nat. Commun. 6 (2015).

[45] Y.Q. Cheng, H.W. Sheng, E. Ma, Relationship between structure, dynamics, and mechanical properties in metallic glass-forming alloys, Phys. Rev. B 78 (2008) 014207.

[46] S.G. Hao, C.Z. Wang, M.Z. Li, R.E. Napolitano, K.M. Ho, Dynamic arrest and glass formation induced by self-aggregation of icosahedral clusters in Zr1-xCux alloys, Phys. Rev. B 84(6) (2011) 064203.